PNAS
www.pnas.org

Supplementary Information for

Targeted Evolution of Pinning Landscapes for Large Superconducting Critical Currents

Ivan A. Sadovskyy, Alexei E. Koshelev, Wai-Kwong Kwok, Ulrich Welp, Andreas Glatz[1]

[1] Email: glatz@anl.gov

This PDF file includes:

- Supplementary text
- Figures S1 to S8
- Captions for Movies S1 to S5

Other supplementary materials for this manuscript include the following:

- Movies S1 to S5

www.pnas.org/cgi/doi/10.1073/pnas.1817417116

Critical dynamics and current-voltage characteristics

Here we study the critical dynamics close to J_c for an array of planar defects in more detail. A snapshot of the order parameter and supercurrent amplitude density is presented in Figure S1. Here, we set the field to $B = 0.1H_{c2}$ and applied a current J slightly larger than critical current J_c, $J = 1.0001J_c$. The depinning process defining the critical current occurs via a collective avalanche process across the sample in a narrow channel in the direction of the Lorentz force (normal to the planar defects). Single vortex motion never occurs; instead, if a vortex depins from one planar defect, vortices from the neighboring defect also need to depin to either free space for the vortex or fill its vacant position. This collective depinning effectively increases the pinning force of the system. The same collective behavior occurs for other types of pinning landscapes, which are *optimized* for highest possible J_c, e.g., for ordered columnar defects (see Ref. [29] in the main text) or disordered nanorods extended along the direction of the applied magnetic field (Ref. [26] in the main text). A similar but somewhat less pronounced effect was observed for randomly placed spherical particles (Ref. [24] in the main text).

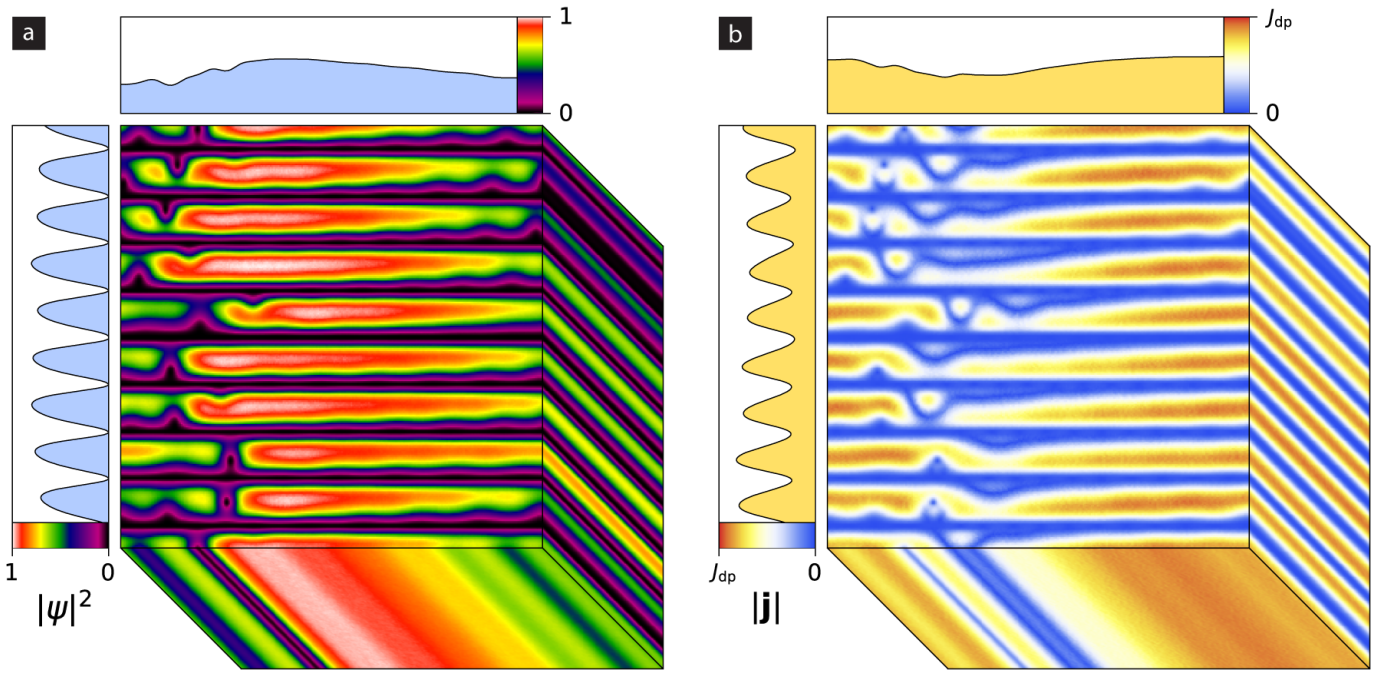

Figure S1. Snapshot of (**a**) the squared order parameter amplitude $|\psi(\mathbf{r})|^2$ and (**b**) supercurrent amplitude $|\mathbf{j}(\mathbf{r})|^2$ for the periodic planar defect configuration in the dynamic/dissipative regime with applied current slightly larger than the critical current at magnetic field $B = 0.1H_{c2}$. The regions occupied by planar defects always have the suppressed order parameter (black horizontal planes in panel **a**) and zero supercurrent (blue planes in panel **b**). The superconductor regions between planar defects have mostly larger order parameter (shown in red and white) interrupted by depinned vortices. Depinning events have distinct, collective behavior, i.e., all vortices depin simultaneous in a certain region spanning through the system almost normal to the planar defects. Due to geometrical constraints of the defects and strong vortex-vortex interaction, vortices do not bend much, which is seen in the depth projection of the system. The corresponding vortex dynamics is shown in Movies S1–S3 for magnetic fields $B = 0.1H_{c2}$, $0.2H_{c2}$, and $0.3H_{c2}$.

The above scenario allows us to conclude that due to the system-spanning clusters of collectively depinning vortices in pinning landscape with very large critical currents, the dynamic transition to the dissipative state tends to be more pronounced and sharper than sub-optimal configurations showing single vortex depinning, as confirmed by the current-voltage (J–E) curves shown in Figure S2a.

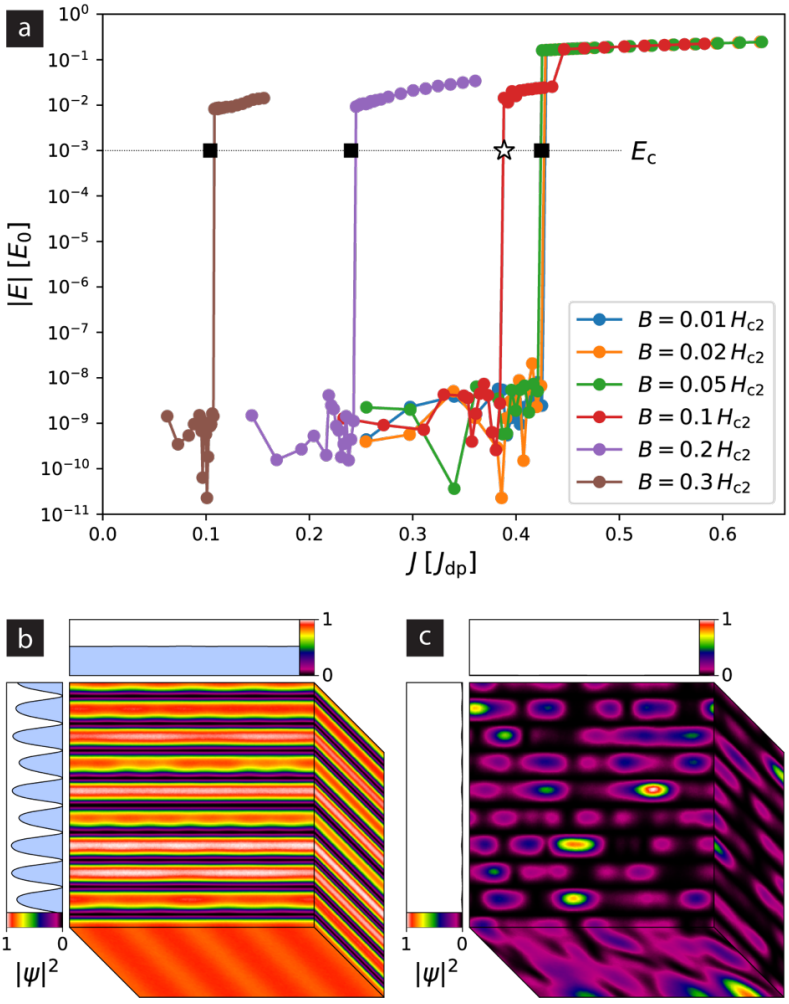

Figure S2. Current-voltage (J–E) curves for the planar defect pinning landscape, which is optimal for field $B = 0.1H_{c2}$, in different applied magnetic fields. In this regime each curve shows an extremely sharp drop (more than 6 orders of magnitude) at the corresponding critical current (black square) determined by the finite voltage criteria $E_c = 10^{-3}E_0$ (dashed line). Voltage levels below $10^{-8}E_0$ cannot be resolved due to numerical noise. **b**. Order parameter amplitude at $B = 0.05H_{c2}$ and current slightly below the critical current, $J = 0.9999J_c$ showing the superconducting state, see also Movie S4. **c**. Order parameter amplitude at $B = 0.05H_{c2}$ and current slightly above critical current, $J = 1.0001J_c$ shows suppressed superconductivity with localized superconducting regions, see also Movie S5.

Here, the various J–E curves are associated with different applied magnetic fields, B, for the same pinning landscape, which was optimized for maximum J_c at $B = 0.1H_{c2}$. Each curve displays a sharp transition with relative voltage drop of at least 10^{-6} around its critical current shown by a star in the data for $B = 0.1H_{c2}$ and black squares for other B values. Note that for lower magnetic fields ($B \lesssim 0.05H_{c2}$), the superconducting state with pinned vortices at $J < J_c$ (Figure S2b) transits directly to a dissipative state consisting of only localized superconducting regions for $J > J_c$ (Figure S2c), which cannot pass a supercurrent through the system, hence bypassing the dissipative superconducting state.

Such sharp transitions allow, in particular, the use of a finite-voltage criterion to determine J_c with rather high threshold electric field, E_c, as shown by the horizontal dashed line in Figure S2a. This threshold field can be 6 to 9 orders of magnitude larger than the 1 μV criterion typically used in experiments, which dramatically reduces the computation time for a single J_c estimation.

List of movies

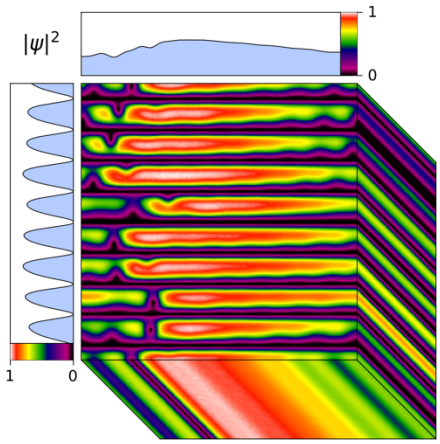

movie-S1.mp4 for $B = 0.1H_{c2}$

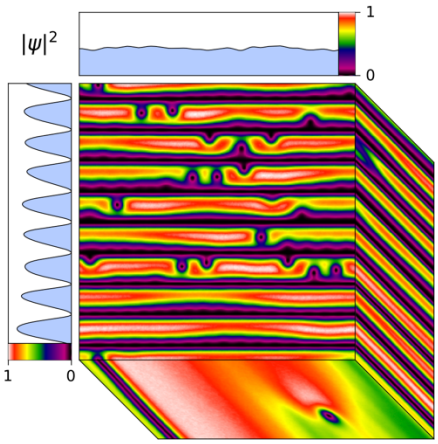

movie-S2.mp4 for $B = 0.2H_{c2}$

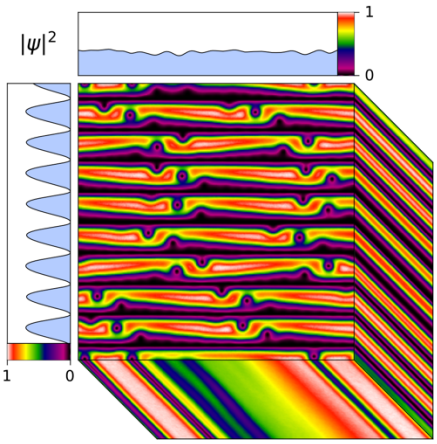

movie-S3.mp4 for $B = 0.3H_{c2}$

Vortex dynamics in the pinning landscape containing planar defects optimized for a magnetic field of $0.1H_{c2}$ in different applied magnetic fields, $0.1H_{c2}$, $0.2H_{c2}$, and $0.3H_{c2}$. The two panels in the movie clips show the squared order parameter amplitude $|\psi(\mathbf{r})|^2$ and supercurrent amplitude $|\mathbf{j}(\mathbf{r})|^2$ for applied current slightly larger than critical current and low temperature (low Langevin noise) regime.

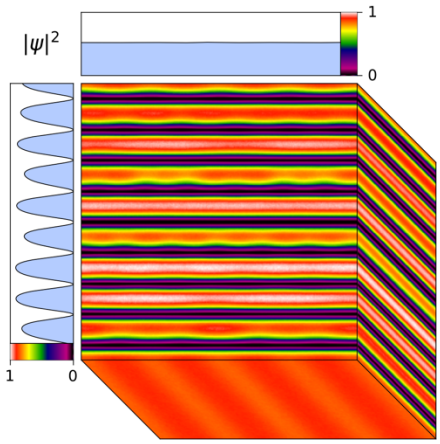

movie-S4.mp4 for $B = 0.05H_{c2}$

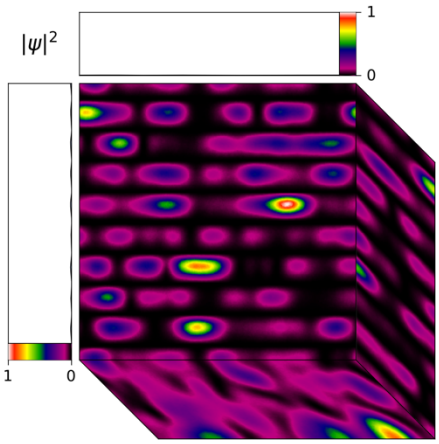

movie-S5.mp4 for $B = 0.05H_{c2}$

Movie clips show the squared order parameter amplitude $|\psi(\mathbf{r})|^2$ and supercurrent amplitude $|\mathbf{j}(\mathbf{r})|^2$ in the superconductor with a pinning landscape consisting of planar defects optimized for magnetic field $0.1H_{c2}$. The applied field is $0.05H_{c2}$. The current slightly below the critical current, $J = 0.9999J_c$, generates a superconducting state with pinned vortices (left). The current slightly above critical current, $J = 1.0001J_c$, shows suppressed superconductivity with localized superconducting regions (right).

Time-Dependent Ginzburg-Landau model

To model vortex dynamics in the superconductor, we solve the dimensionless TDGL equation,

$$(\partial_t + i\mu)\psi = \varepsilon(\mathbf{r})\psi - |\psi|^2\psi + (\partial_\mathbf{r} - i\mathbf{A})^2\psi + \zeta(\mathbf{r}, t),$$

for the complex order parameter $\psi(\mathbf{r}, t)$ in the infinite-λ limit. We evolve a system of size $64\xi \times 64\xi \times 8\xi$ with grid spacing of 0.5ξ and quasi-periodic boundary conditions in each direction. Here, $\mu = \mu(\mathbf{r})$ is the electric scalar potential, $\mathbf{A}$ the vector potential associated with the external magnetic field $\mathbf{B} = \mathrm{curl}\,\mathbf{A}$, and $\zeta(\mathbf{r}, t)$ is the temperature-dependent δ-correlated Langevin term. The unit of length is the superconducting coherence length $\xi = \xi(T)$ at a given temperature T, the unit of magnetic field is the upper critical field, $H_{c2} = H_{c2}(T) = \hbar c/2e\xi^2$, the unit of the current density,

$$\mathbf{J} = (3^{3/2}/2)\,\{\mathrm{Im}[\psi^*(\partial_\mathbf{r} - i\mathbf{A})\psi] - \partial_\mathbf{r}\mu\},$$

is the depairing current, $J_{dp} = J_{dp}(T)$, and the unit of electric field is $E_0 = (3^{3/2}/2)J_{dp}/\sigma$, where σ is the normal-state conductance.

For the samplings shown in Figure 3 in the main text and Figures S4–S8 as well as for the conventional optimization in Figure 3a in the main text we use a system of size $128\xi \times 128\xi \times 128\xi$. In the scenario shown in Figure 4c of the main text we used a $32\xi \times 32\xi \times 32\xi$ simulation box.

In order to determine the critical current density, J_c, we utilize a finite-electrical-field criterion. Technically, we adjust the applied external current to reach certain electrical-field level across the system. By targeting a small threshold electrical-field level $E_c = 10^{-3}E_0$ and averaging over steady state long enough we obtain a critical current, see Refs. [25, 35] in the min text for details.

In simulations we parametrize real temperature, T, and critical temperature map, $T_c(\mathbf{r})$ using two dimensionless quantities: linear term coefficient,

$$\varepsilon(\mathbf{r}) = [T_c(\mathbf{r}) - T] \,/\, [T_{c,b} - T],$$

and noise-level coefficient, $T_f \propto T$, in Langevin term, $\zeta(\mathbf{r}, t)$.

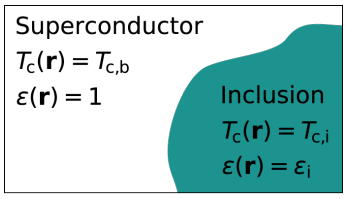

Figure S3. Sketch of a critical temperature map.

We model non-superconducting inclusions with a reduced critical temperature, $T_{c,i}$, inside each defect ellipsoid, resulting in a suppressed Ginzburg-Landau order parameter inside these inclusions. Typically, we use almost zero $T_{c,i}$ corresponding to the suppressed order parameter in the entire inclusion region. Technically, we set a very negative coefficient before linear term, $\varepsilon_i = (T_{c,i} - T)/(T_{c,b} - T) = -30$, where we set $1 - T/T_{c,b} = 1/31$ is the critical temperature in the bulk superconductor and $T = T_{c,b}$ is a system temperature. In the plots below we compare this situation to weaker pinning centers having $\varepsilon_i = -1$ corresponding to $T_{c,i} = 2T - T_{c,b}$.

The temperature-induced noise is modelled by the additive Langevin term, $\zeta(\mathbf{r}, t)$, in the TDGL equation with correlator $\langle\zeta^*(\mathbf{r}, t)\,\zeta(\mathbf{r}', t')\rangle = T_f\,\delta(\mathbf{r} - \mathbf{r}')\,\delta(t - t')$, see Ref. [35] in the min text for details. In the plots below, we compare the low-temperature regime, $T = 0$ K, modeled by low Langevin-term coefficient $T_f = 10^{-5}$ to the high-temperature regime, $T = 77$ K, having high Langevin coefficient $T_f = 0.28$.

Sampling

Planar vs. Columnar defects at 0 K

In order to understand why the planar defects give a larger critical current compared to columns with circular cross section, we consider an isolated cylindrical defect of elliptical cross-section defined by main axes a and b. We apply an average current density J along a and a magnetic field along the cylinder. The *local* current density at the depinning point (at the extremal points of the defect boundary along b) is $J_l = J(a + b)/a$; for columnar defects with circular cross-section $J_l = 2J$, while for planar defects this value is twice smaller, $J_l = J$. It means that for defect, the depinning force is expected to be roughly twice larger for planar defect for the same average current density. In the case of an ordered pattern of defects the situation is more complicated.

In Figures S4–S6 we provide a sampling set of J_c for the hexagonal lattice made of columnar defects with cross-section a and b for a/b ratios ranging from planar defects ($a \to \infty$) to cylindrical columns ($a = b$). Figures S7–S8 demonstrate the influence of the randomness in the defect placement. All plots are for a current applied in x direction and magnetic field of $B = 0.1H_{c2}$ directed along the z axis.

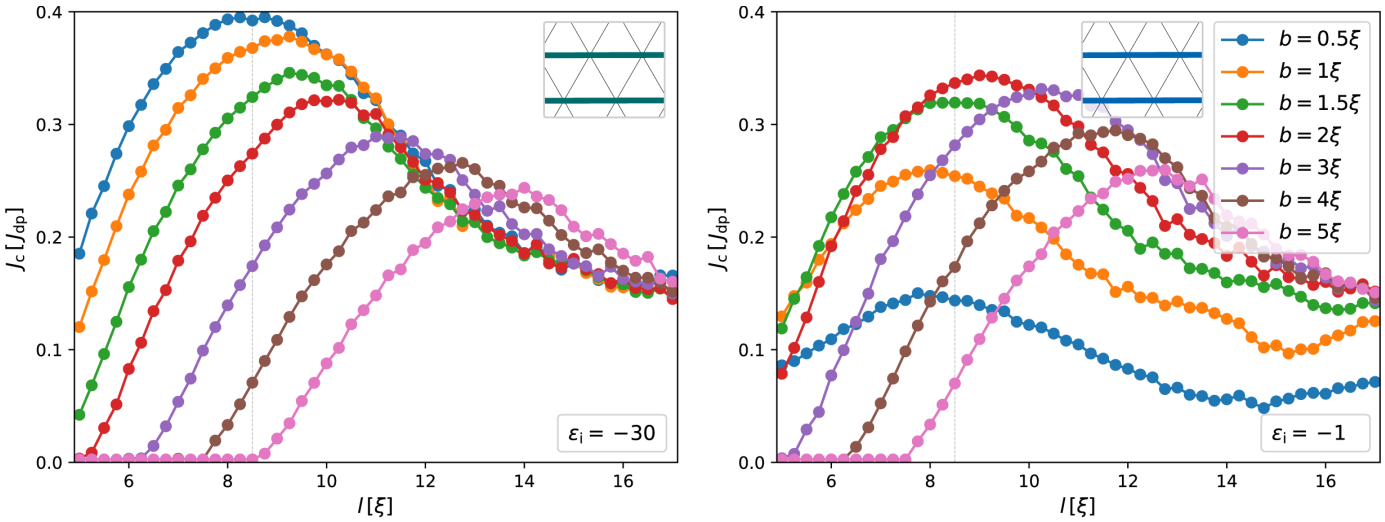

Figure S4. Critical current J_c for walls in xz plane as a function of associated lattice constant l (proportional to the distance between walls $l = 2d/3^{1/2}$) for different wall thickness b in the cases of strong ($\varepsilon_i = -30$, left) and weak ($\varepsilon_i = -1$, right) pinners. A small Langevin noise coefficient is used corresponding to near-zero temperatures.

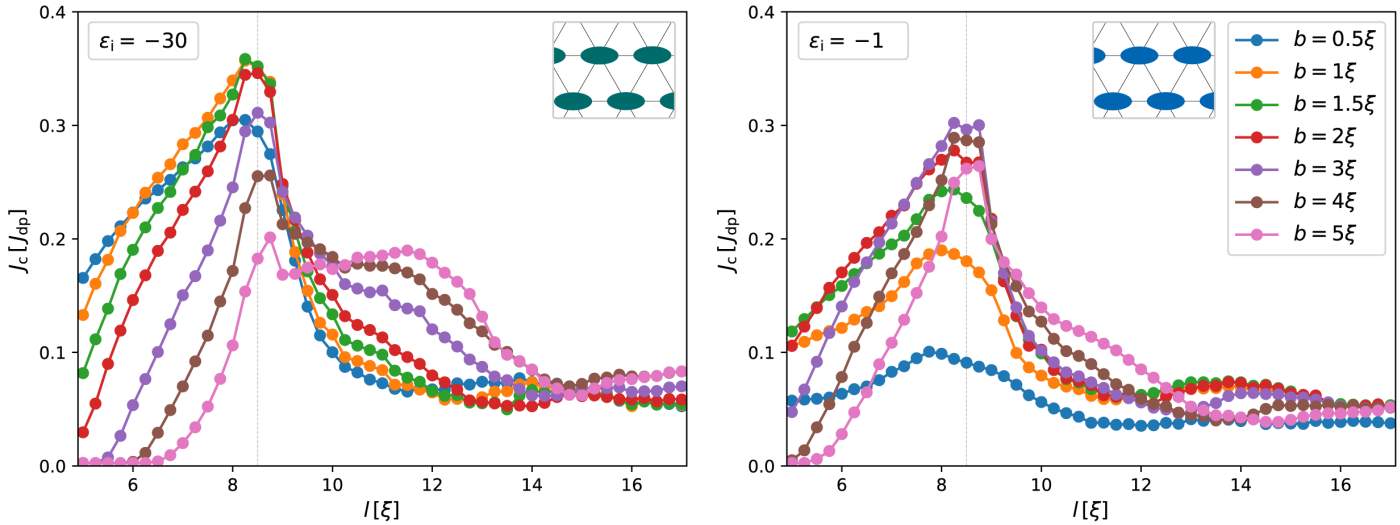

Figure S5. Critical current J_c for hexagonal lattice of columnar defects with elliptical cross-section *ab* (*a* is in *x* direction, *b* is in *y* direction) as a function of lattice constant *l* for a = 4ξ and different *b* in the cases of strong ($\varepsilon_i = -30$, left) and weak ($\varepsilon_i = -1$, right) pinners. A small Langevin noise coefficient is used corresponding to near-zero temperatures.

Circular-shaped columnar defects ordered in hexagonal lattice at 0 K and 77 K

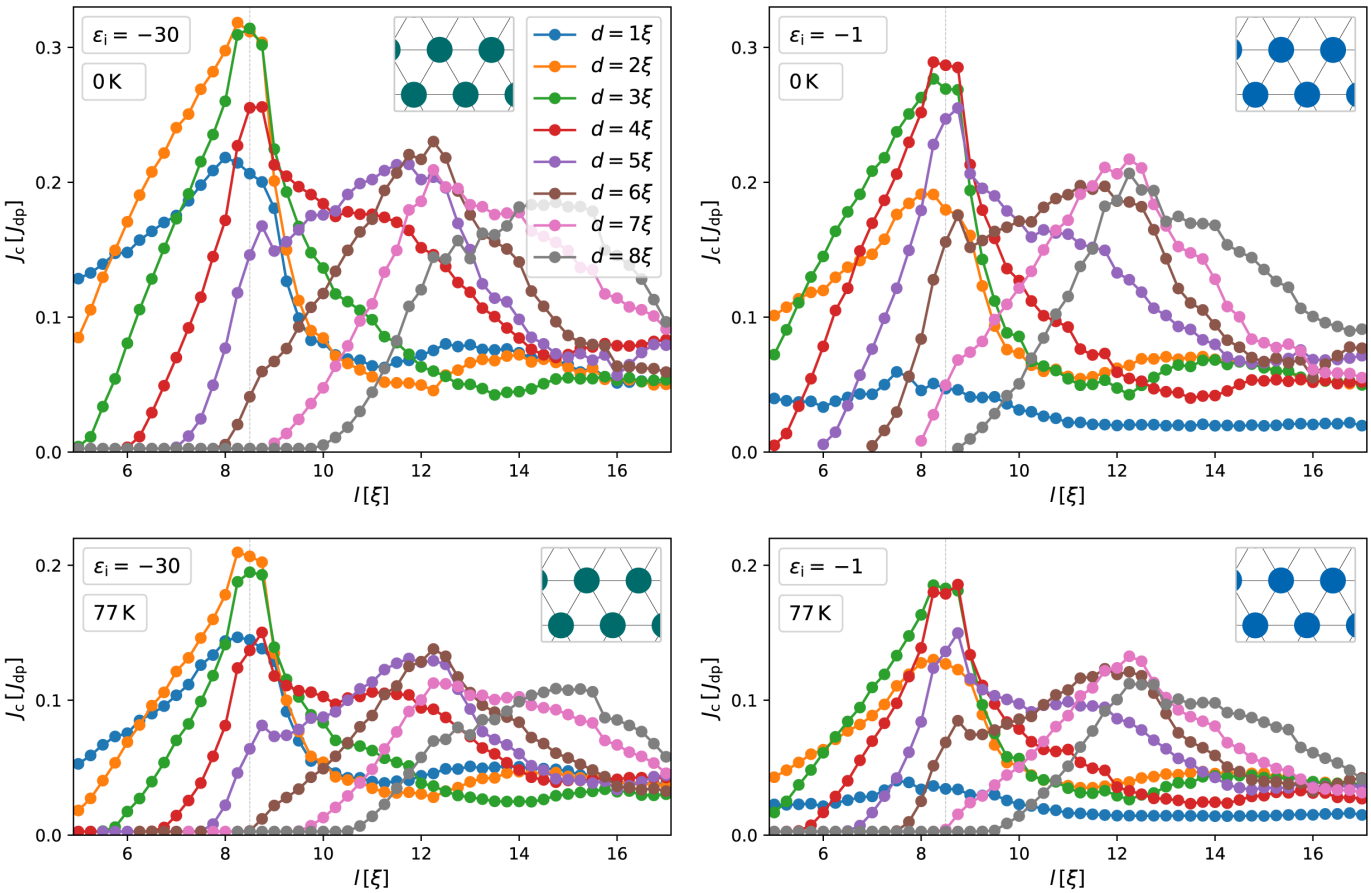

Figure S6. Critical current J_c for hexagonal lattice of columnar defects with circular cross-section of dimeter d as a function of lattice constant l for different d in the cases of strong ($\varepsilon_i = -30$, left) and weak ($\varepsilon_i = -1$, right) pinners. Both are shown for two different temperatures: small Langevin noise coefficient ($T_f = 10^{-5}$) corresponding to near-zero temperatures (top row) and larger noise coefficient ($T_f = 0.28$) corresponding to 77 K (bottom row).

Elliptically-shaped columnar defects ordered in hexagonal lattice at 0 K and 77 K

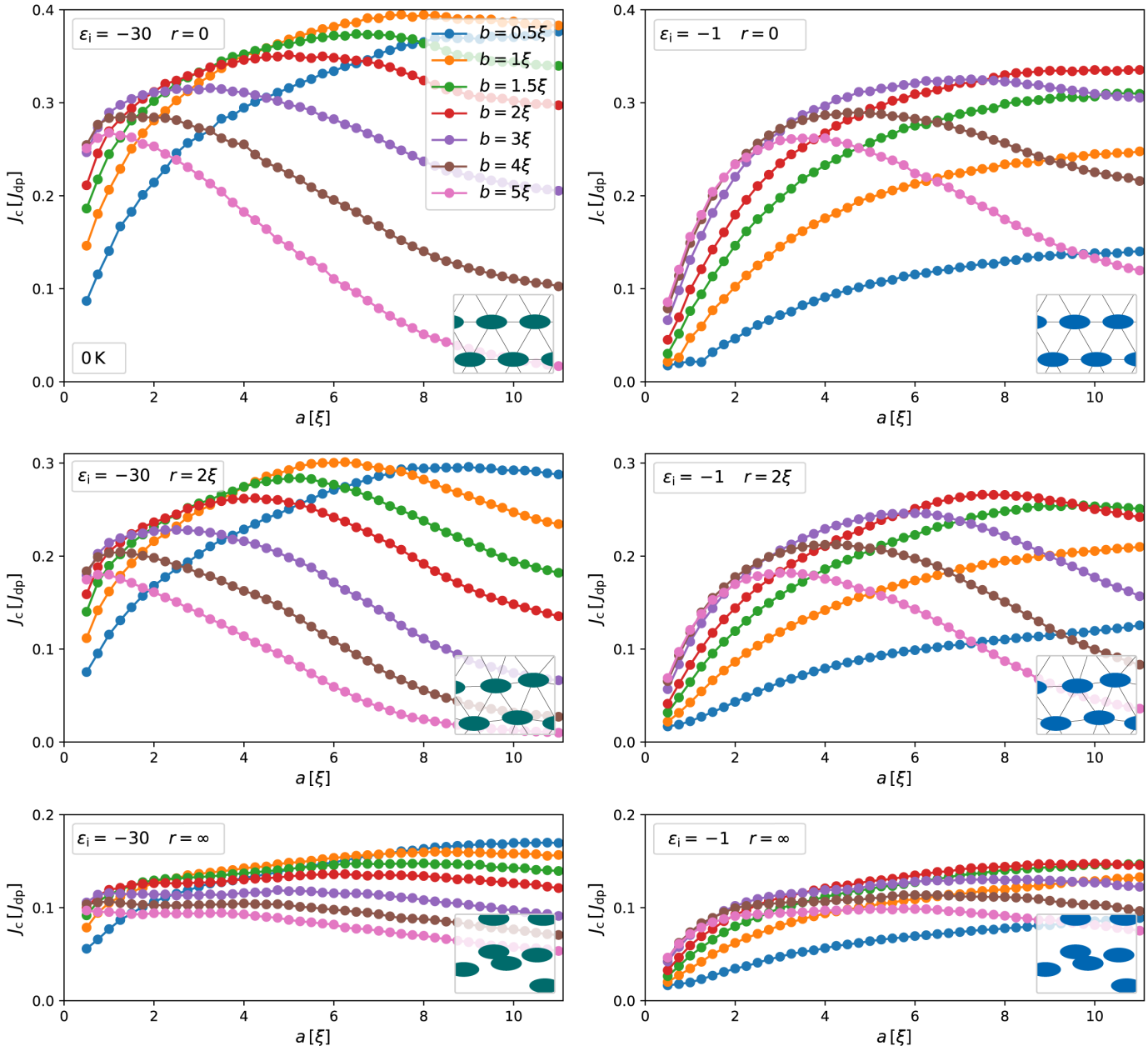

Figure S7. Critical current J_c for hexagonal lattice of columnar defects with elliptical cross-section *ab* (*a* is in *x* direction, *b* is in *y* direction) as a function of *a* for lattice constant $l = 8.5\xi$ and different *b*. Some randomness, *r*, is added to the *x* and *y* positions of the defects, i.e. δx, $\delta y = [-r, \ldots, r]$. Shown for a perfect hexagonal lattice with $r = 0$ (top row), lattice with intermediate randomness having $r = 2\xi$ (medium row), and uncorrelated placement of defects corresponding to $r = \infty$ (bottom row). Strong ($\varepsilon_i = -30$, left column) and weak ($\varepsilon_i = -1$, right column) pinners. A small Langevin noise coefficient is used ($T_f = 10^{-5}$) corresponding to near-zero temperatures.

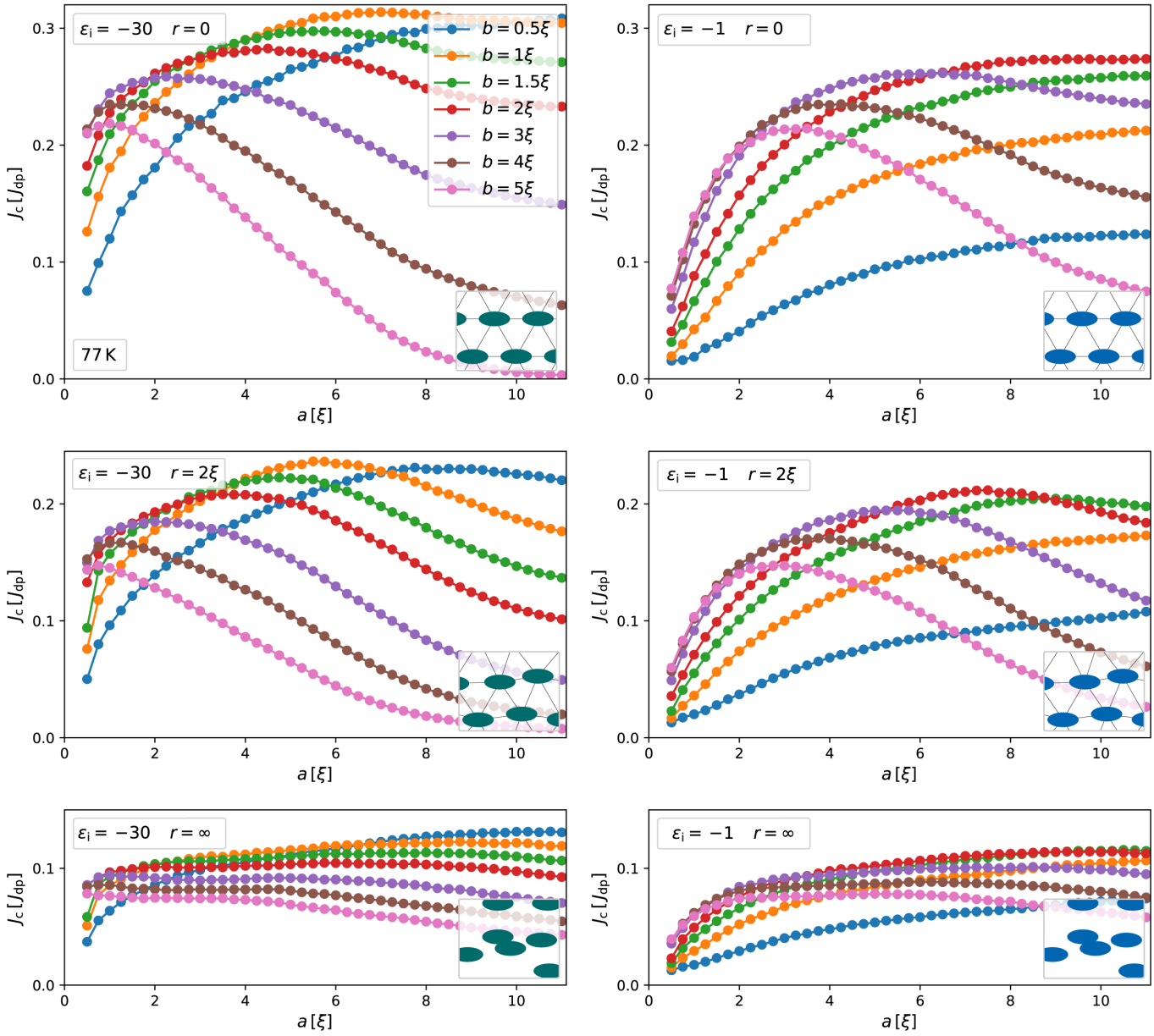

Figure S8. The same as in Figure S7 but for larger Langevin noise coefficient (T_f = 0.28) corresponding to 77 K.

Details of numerical simulations

We have implemented the time-dependent Ginzburg-Landau (TDGL) solver on General Purpose Graphics Processing Units (GP GPUs) using the CUDA framework and used Python for the evolutionary algorithm and job control on specialized computational clusters. The results of the evolution of different types were obtained on Titan, a Cray XK7 supercomputer at Oak Ridge Leadership Computing Facility running NVIDIA Kepler GPUs. We parallelized the computations running 16–256 pinning landscapes in one generation.

We also used the high-performance GPU clusters GAEA at Northern Illinois University and Cooley at the Argonne Leadership Computing Facility for extrapolation, analysis, and visualizing the results.